Magnetic light amplification by stimulated emission of radiation in subwavelength systems of a dielectric cavity and magnetic quantum emitters

Zhong-Jian Yang [ORCID],[*] Xiao-Jing Du, Ma-Long Hu, and Jun He [ORCID][†]

Hunan Key Laboratory of Nanophotonics and Devices, School of Physics and Electronics,
Central South University, Changsha 410083, China

We propose a magnetic laser in a subwavelength system consisting of a high-refractive-index dielectric cavity and an active medium formed by magnetic quantum emitters. Stimulated emissions of magnetic quantum emitters induced by their coherent interactions with quantized magnetic fields of a cavity are theoretically considered. The condition to achieve such a magnetic laser is obtained. Numerical results show that magnetic lasers are feasible in some realistic systems, for example, a silicon disk of high-quality whispering gallery modes with embedded emitters. Furthermore, the competitions between the electric interaction and magnetic one in terms of their Purcell factors are also considered in some magnetic laser achievable systems. In a wavelength-scale silicon block of a high-order magnetic mode, the ratio of magnetic Purcell factor to the electric one can reach more than $\sim 10^3$ large. Our results open up ways to enhanced magnetic light-matter interactions.

I. INTRODUCTION

The interactions of the magnetic component of light and magnetic dipole (MD) transitions at optical frequencies are usually several orders of lower than their electric counterparts [1,2]. Hence, the light-matter interactions are generally interpreted as the couplings of electric fields and electric dipoles. Nevertheless, the magnetic interactions provide another dimension in glimpsing light-matter interactions [2–4]. Furthermore, strong MD transitions of quantum emitters at optical frequencies are indeed found in some lanthanide series ions such as Eu^{3+} and Er^{3+} [5–7]. The interactions of these magnetic quantum emitters (MQEs) with light have been attracting increasing research interests despite high technology requirements [4,8–12].

Putting MQEs close to photonic structures could allow one to largely turn the couplings between MQEs and light. The spontaneous decay-rate enhancement, which is also termed as Purcell factor [13–15], can be modified a great deal [4]. Due to their high near-field confinement, plasmonic nanostructures have been utilized to interact with MQEs [4,16–18]. However, plasmonic systems suffer from high material losses, and complex geometries are required to obtain effective magnetic responses. In the past years, all-dielectric (sub)wavelength-scale structures with high-refractive indexes n_r have been found to exhibit Mie-like resonances [19,20], and they can readily support magnetic near-field responses. Those magnetic responses provide a platform for magnetic light-matter interactions [21–24]. The common resonant modes in the reported subwavelength all-dielectric structures are low-order electromagnetic multipoles such as electric/magnetic dipoles, toroidal modes, and supercavity mode [19,20,25–28].

Most of these modes show low-quality (Q) factors ($\sim 10^1$) and low electromagnetic near field enhancement ($\sim 10^1$) with a common material silicon (Si), $n_r \sim 3.5$. Recently, it has been demonstrated that subwavelength dielectric resonators ($n_r \sim 3.5$) can also support whispering-gallery modes (WGMs) with high enough Q factors ($\sim 10^5$) and high electromagnetic near field enhancements ($\sim 10^2$) [29]. These achievements of all-dielectric magnetic cavities hold great promise to enable more efficient magnetic photons-MQEs couplings [30,31].

Here, we theoretically propose that a magnetic laser can be obtained in a subwavelength system of a dielectric cavity and MQEs. MQEs are modeled as simple two-level emitters with MD transitions. The MQEs can undergo stimulated emission of radiation though coherent interactions with the photons in the cavity. The stimulated emission is similar to that in common lasers or spasers [32–40], while the couplings here are magnetic interactions instead of the electric ones. A subwavelength dielectric disk with high-Q WGMs is numerically considered. The magnetic laser can be obtained due to the high-Q features of the WGMs. Furthermore, we also consider the competition between the magnetic interactions and electric ones in some magnetic laser achievable systems. Specifically, the ratio of magnetic Purcell factor to the electric one in a subwavelength silicon block of a high-Q magnetic mode can reach $\sim 10^3$ large. This property makes such a kind of dielectric cavity a suitable platform to carry out the magnetic light-matter interactions including a magnetic laser.

II. THEORETICAL APPROACH

The magnetic field of a high-Q resonant mode of a dielectric cavity can be quantized based on that of the standard harmonic oscillators [37,41,42] (see Appendix A). A MQE is taken as a two-level emitter with a matrix element of $\tilde{M}_{10}$ for

[*]zjyang@csu.edu.cn
[†]junhe@csu.edu.cn

its MD transition. Then, the interaction Hamiltonian between a MQE and the quantized magnetic field under the rotating-wave approximation can be expressed as

$$H_{\text{int}} = \hbar g(\hat{a}\hat{\sigma}_{10}e^{-i[\omega_n t + \varphi(r)]} + \hat{a}^+\hat{\sigma}_{01}e^{i[\omega_n t + \varphi(r)]}), \quad (1)$$

where ω_n is the frequency of the photon, and $\hat{a}^+$ and $\hat{a}$ are the creation and annihilation operators of a photon, respectively. $\hat{\sigma}_{10}$ and $\hat{\sigma}_{01}$ are transition operators of the MQE. $\varphi(r)$ represents the spatial phase of the magnetic field at the location r. g is the coupling strength $g = \sqrt{\frac{\mu_0\omega n}{2\hbar V m}}\overrightarrow{M}_{10} \cdot \frac{\vec{B}(r)}{B_{\max}}$ (see Appendix A), where V_m is the magnetic field mode volume of the cavity $V_m = \frac{\int \mu_0|\vec{H}(r)|^2 d^3r}{\mu_0 H_{\max}^2}$, $\vec{B}(r)/B_{\max}[= \vec{H}(r)/H_{\max}]$ is the normalized magnitude of the magnetic field in the cavity, $\vec{H}(r)$ is the magnitude of the magnetic field at location r, $\hbar$ is reduced Planck constant, and μ_0 is the permeability of vacuum. The analytical description is similar to that of electric interactions [38,43–46], while the coupling strength g should be replaced by $g_e = \sqrt{\frac{\omega n}{2\hbar\varepsilon_0 V_e}}\overrightarrow{\mu}_{10} \cdot \frac{\vec{E}(r)}{E_{\max}}$ for an electric interaction. $\vec{\mu}_{10}$ is the matrix element of the electric dipole transition of an electric quantum emitter (EQE), $\vec{E}(r)/E_{\max}$ is the normalized electric field, ε_0 is the permittivity of vacuum, and V_e is the electric-field mode volume of a cavity mode.

Under Fermi's golden rule, the total emission rate into photons from a MQE can be expressed as (see Appendix B)

$$\Gamma' = 2\pi g^2 (N_n + 1) \int F(\omega)\frac{\gamma_n^2}{(\omega - \omega_n)^2 + \gamma_n^2}d\omega, \quad (2)$$

where the term $N_n + 1$ represents the contributions from the stimulated Γ^{st} (N_n) and spontaneous Γ^{sp} (1) emissions. $\int F(\omega)\frac{\gamma_n^2}{(\omega-\omega_n)^2+\gamma_n^2}d\omega$ is the spectral overlap factor [37], where $F(\omega)$ is the normalized-to-1 spectrum of MD transitions, and γ_n is the relaxation rate of the photon. $F(\omega)$ is highly related to the relaxation rate (γ_{10}) of the MQE. For $\gamma_{10} \ll \gamma_n$, the overlap factor is 1. While for $\gamma_{10} \gg \gamma_n$, the overlap factor becomes γ_n / γ_{10}. Note that in the above integrations of overlap factors, we have assumed the resonant couplings between the MQE and photons. The stimulated absorption rate Γ^{sa} is equal to the stimulated emission rate $\Gamma^{\text{sa}} = \Gamma^{\text{st}}$. For the couplings of many MQEs and photons, the generation rate of photon number N_n can be expressed as

$$\dot{N}_n = \int \Gamma^{\text{st}}\rho_{\text{eff}}(r)d^3r + \int \Gamma^{\text{sp}}\rho_1(r)d^3r - N_n\gamma_n \quad (3)$$

where $\rho_{\text{eff}}(r) = \rho_1(r) - \rho_0(r)$, $\rho_1(r)$ and $\rho_0(r)$ are the population densities of MQEs in the excited and ground states, respectively. The rate equation for the population of MQEs can be written as (see Appendix C)

$$\int \dot{\rho}_{\text{eff}}(r)d^3r = \int (W_{01} - \Gamma^{\text{sp}})(\rho_1(r) + \rho_0(r))d^3r$$
$$- \int (W_{01} + \Gamma^{\text{sp}} + 2\Gamma^{\text{st}})\rho_{\text{eff}}(r)d^3r, \quad (4)$$

where W_{01} is the pumping rate of the MQEs.

The coupling strength g is an important parameter that determines if a magnetic laser can be realized in a system. Generally, g can be obtained by calculating the mode

volume based on numerical methods, for example, the finite-difference time- domain (FDTD) simulations. Alternatively, the spontaneous decay rate enhancement can be simulated by numerical methods. Then, g can also be obtained correspondingly. In the FDTD simulations, the calculations are carried out with the condition of $\gamma_{10} \ll \gamma_n$, and the directly simulated decay rate enhancement is $2\pi g^2/\Gamma_1$, where Γ_1 is the decay rate of a MQE in the medium of n_r [31]. $\Gamma_1 = n_r^3\Gamma_0$, where Γ_0 is the vacuum spontaneous decay rate of a MQE [4]. Thus, the magnetic Purcell factor is $\Gamma^{\text{sp}}/\Gamma_0 = 2\pi g^2/\Gamma_0 = 2\pi g^2 n_r^3/\Gamma_1$.

In our considered systems, a photon is generated through stimulated or spontaneous emission from MQEs. Meanwhile, a photon can be annihilated through stimulated absorption by MQEs or its own relaxation in the cavity [Eq. (3)]. The net generation rate of coherent photons in a system is $\int \rho_{\text{eff}}(r)\Gamma^{\text{st}}d^3r$. The magnetic laser can occur when this value is larger than the photon relaxation rate $N_n\gamma_n$, namely,

$$\int \rho_{\text{eff}}(r)\Gamma^{\text{st}}d^3r > N_n\gamma_n. \quad (5)$$

If we assume that the coupling strength g of each MQE and cavity is the same for simplicity. Under the situation of $\gamma_{10} \ll \gamma_n$, the net generation rate of coherent photons becomes $N_{\text{eff}}\Gamma^{\text{st}}$. Here, N_{eff} is the inversed total number of MQEs $N_{\text{eff}} = \int \rho_{\text{eff}}(r)d^3r$. Eq. (5) then reduces to

$$N_{\text{eff}}2\pi g^2 > \gamma_n. \quad (6)$$

Thus, $\gamma_n/2\pi g^2$ represents the threshold number of MQEs required to achieve a magnetic laser in the above-considered system. Under the situation of $\gamma_{10} \gg \gamma_n$, the net generation rate of coherent photons is $N_{\text{eff}}\Gamma^{\text{st}} \gamma_n/ \gamma_{10}$. The condition to realize a magnetic laser becomes $N_{\text{eff}}2\pi g^2 > \gamma_{10}$ correspondingly. For the rest of discussion, we will take the situation of $\gamma_{10} \ll \gamma_n$ unless specified.

III. MAGNETIC LASER IN A SUBWAVELENGTH WGM CAVITY

A realistic dielectric cavity with active MQEs is considered as shown in Fig. 1(a). The cavity is a Si disk support-ing high-Q subwavelength WGMs [29]. The radius and the height are both 630 nm. The geometry is chosen to match the wavelength region such that the refractive index of Si is around $n_r = 3.5$. Simulations show that the resonance of a TE WGM of the azimuthal mode index $m = 7$ occurs at $\lambda = 1230$ nm. The Q factor of this mode is 1.5×10^5 and the corresponding relaxation rate is $\gamma_n = 1.6 \times 10^9$ s^{-1}. The magnetic Purcell factor $2\pi g^2/\Gamma_0$ can reach 1.65×10^5. Note that the diameter of the above disk is very close to the resonant wavelength of $m = 7$ mode, while the height is much smaller than this wavelength. Thus, one can roughly take this mode as a subwavelength resonance. In fact, by slightly increasing the height and decreasing the diameter, a WGM mode will keep the same resonant wavelength and almost the same Q factor, while both the diameter and height are completely subwavelength [29]. In this work, the height and radius are taken the same for simplicity.

We assume the maximum population inversion of active MQEs $\rho_1 \gg \rho_0$. Thus, $N_{\text{eff}} \approx N_{\text{MQE}} = \int (\rho_1(r) + \rho_0(r))d^3r$, where N_{MQE} represents the total number of MQEs. The
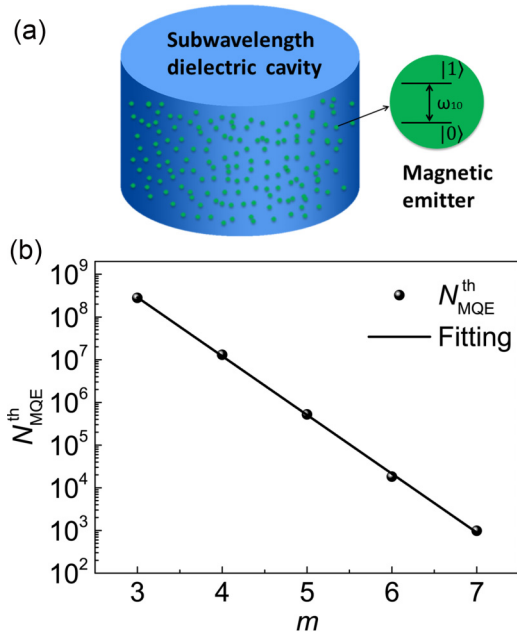
FIG. 1. (a) Schematic of a magnetic laser system consisting of a subwavelength dielectric cavity and active MQEs. Each MQE is a two-level emitter. (b) N_{MQE}^{th} of a WGM-resonant Si cavity with different mode m. Each WGM is a TE mode. The line is the fitting results with an exponential decay function. Radius and height are both 630 nm.

coupling strength g of each MQE and cavity is assumed to be the same for simplicity. With the situation of low enough temperature ($\gamma_{10} \ll \gamma_n$) and a realistic value of $\Gamma_0 = 10^1$ s^{-1} [7], the threshold number of MQEs required to achieve a magnetic laser is $N_{MQE}^{th} \approx \gamma_n/2\pi g^2 \approx 9.8 \times 10^2$ based on Eq. (6). Such a threshold value should be easily satisfied experimentally. The N_{MQE}^{th} for a magnetic laser increases dramatically as the Q factor of a cavity mode decreases [$N_{MQE}^{th} \sim 1/Q^2$, Fig. 1(b)], and reaches more than $\sim 10^8$ for $m = 3$ ($Q \approx 150$). For the situation of $\gamma_{10} \gg \gamma_n$, the N_{MQE}^{th} becomes $N_{MQE}^{th} = \gamma_{10}/2\pi g^2$. This value is relatively γ_{10}/γ_n times larger than that under the situation of low enough temperature.

By enlarging the size of a disk cavity, it becomes relatively easier to obtain a magnetic laser. The WGM response is a geometric resonance in a dielectric cavity. Thus, the resonant wavelength λ_n of a WGM is in proportion to the disk diameter D ($\lambda_n \propto D$) [29], where the height/diameter ratio of a disk is always kept the same. The Q factor of each WGM remains the same with varying the disk size [Fig. 2(a)]. The magnetic field distribution size increases proportionally with the disk size. Thus, the mode volume V_m increases proportionally with the geometric volume of the disk ($V_m \propto D^3$). By combining all these factors, the Purcell factor $\frac{\Gamma^{sp}}{\Gamma_0} = \frac{2\pi g^2}{\Gamma_0} \propto Q\lambda_n^3/V_m$ [4] also remains unchanged with disk size. This is also confirmed by direct simulations [Fig. 2(a)]. The decay rate of a WGM photon γ_n decreases with the disk size $\gamma_n \propto 1/D$ as the resonant frequency ω_n decreases with D ($\omega_n \propto 1/D$), while the Q factor remains unchanged. Thus, the N_{MQE}^{th} to achieve a magnetic laser becomes relatively smaller with disk size $N_{MQE}^{th} = \gamma_n/2\pi g^2 \propto 1/D$ [Fig. 2(b)]. Here, we have assumed a fixed Γ_0 for simplicity. The above analysis is not restricted to
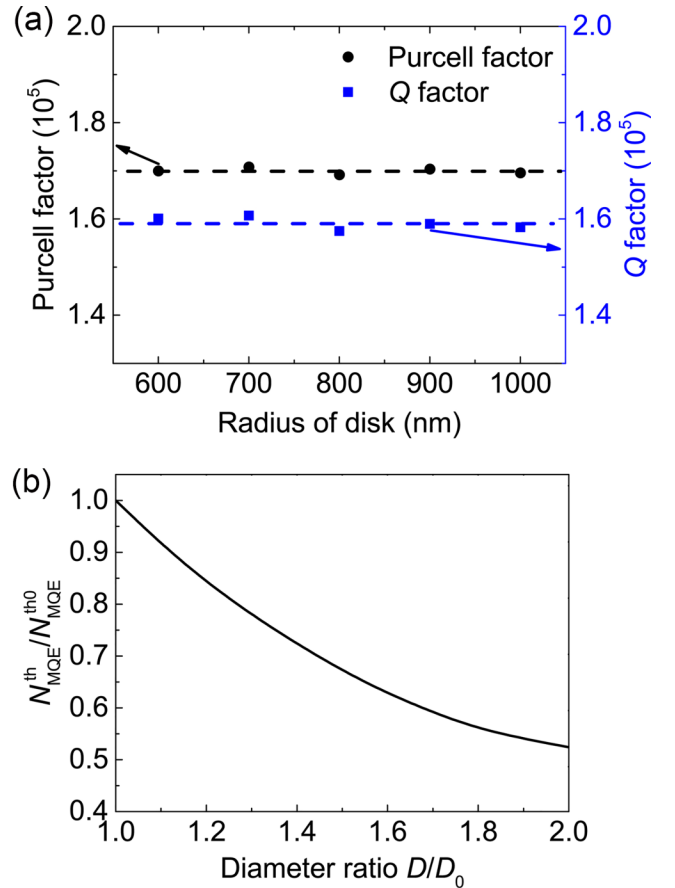

FIG. 2. (a) Directly simulated Q factor (blue dots) and magnetic Purcell factor Γ^{sp}/Γ_0 (black dots) as a function of the disk size (radius). WGM is an $m = 7$ TE mode for each case. (b) Normalized threshold number of MQEs $N_{MQE}^{th}/N_{MQE}^{th0}$ as a function of the size (diameter) ratio D/D_0 (red line). D_0 is a reference diameter of a disk with a threshold number of N_{MQE}^{th0}. Height is always kept the same for the radius in each case.

a specific WGM. Thus, the relation $N_{MQE}^{th} \propto 1/D$ with a fixed Γ_0 applies for any WGM in the disk system. Furthermore, a larger disk also provides more space to host the MQEs. This is also an important profitable factor to realize such a system in experiments.

Now, let us turn to the number of photons N_n of the magnetic laser system. At first, N_n increases as the gain is larger than the loss. Then, N_n turns to be saturated (denoted by N_n^{max}) when the gain equals the loss. The N_n^{max} can be obtained by solving Eqs. (3) and (4) under the steady-state conditions, namely, $\dot{\rho}_{eff} = 0$ and $\dot{N}_n = 0$. The analytical expression of N_n^{max} as a function of the system parameters is complex (see Appendix D). There are two solutions for N_n^{max}, where the negative one is omitted. The N_n^{max} as a function of pumping rate for cases with different number of MQEs N_{MQE} are shown in Fig. 3. When N_{MQE} is more than several times larger than the N_{MQE}^{th}, N_n^{max} increases linearly with the pumping rate W_{01} ($N_n^{max} \propto (N_{MQE} - N_{MQE}^{th})W_{01}/\Gamma^{sp}$). For the case where N_{MQE} is equal to the N_{MQE}^{th}, N_n^{max} shows a square-root function of the pumping rate $N_n^{max} = \sqrt{\frac{W_{01}}{2\Gamma^{sp}} + \frac{1}{4}} - \frac{1}{4}$.
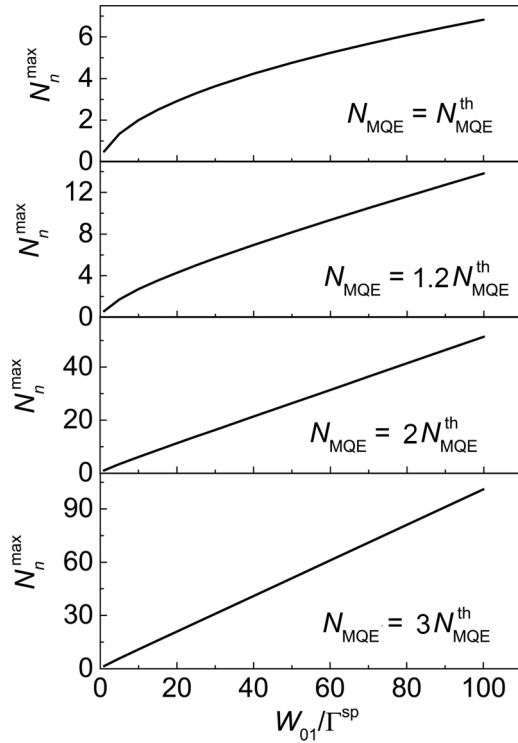
FIG. 3. Saturated number of photons N_n^{max} as a function of the normalized pumping rate W_{01}/Γ^{sp}. Number of MQEs N_{MQE} varies from N_{MQE}^{th} to $3N_{MQE}^{th}$.

IV. COMPETITIONS BETWEEN MAGNETIC AND ELECTRIC INTERACTIONS

We shall now investigate the coupling strengths of a magnetic interaction and an electric interaction associated with a cavity mode. This is an important factor that determines if a magnetic laser action can exceed an electric one. Note that Eq. (6) also holds for the electric case, while the $2\pi g^2$ term should be replaced by $2\pi g_e^2$ to represent the electric interaction. The Purcell factor of an EQE can be expressed as Γ_e^{sp}/Γ_0^e, where Γ_e^{sp} and Γ_0^e are the spontaneous decay rate of an EQE in a cavity and vacuum, respectively. The ratio of the vacuum decay rate of an EQE to that of a MQE Γ_0^e/Γ_0 can reach several orders of magnitude for a common molecular, while it can be much smaller for a rare-earth ion [5,6]. We assume resonant couplings for both electric and magnetic interactions. Numerical calculations show that the $\frac{\Gamma^{sp}/\Gamma_0}{\Gamma_e^{sp}/\Gamma_0^e}$ is $\sim 10^1$ for a WGM of $n_r = 3.5$ (Fig. 4). This means that Γ_0^e/Γ_0 should be smaller than $\sim 10^1$ to make the magnetic interaction stronger than the electric one. This can be realistic for rare-earth ions if only the magnetic interaction is a resonant coupling. The detuning of the nonresonant electric interaction is $\omega - \omega_n = f\gamma_n$. Based on Eq. (2), the nonresonant decay rate of an emitter is $1/(f^2 + 1)$ times of the resonant one. This will make the ratio $\frac{\Gamma^{sp}/\Gamma_0}{\Gamma_e^{sp}/\Gamma_0^e}$ become relatively $(f^2 + 1)$ times larger.

One efficient way to further enlarge the emission ratio $\frac{\Gamma^{sp}/\Gamma_0}{\Gamma_e^{sp}/\Gamma_0^e}$ can be considered by putting an emitter inside a less symmetrical cavity. Here, we also assume resonant couplings for both electric and magnetic interactions for simplicity. Figure 5(a) shows a Si block cavity with an emitter at its
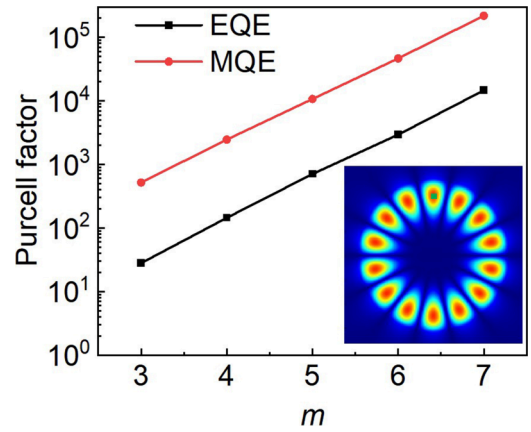

FIG. 4. Magnetic Purcell factors for different modes (red dots). Electric Purcell factors with an EQE as the excitation are also shown (black dots). Disk is the same as that in Fig. 1(b). For each case, an emitter is placed at the maximal field of a mode. Inset shows magnetic field distribution at the center cross section of the disk ($m = 7$). A MQE denoted by the green point is located at a maximal field point of the $m = 7$ WGM mode.

center. The length, width, and height are 1500, 1050, and 1050 nm, respectively. Here, the size of the cavity is also chosen to match that n_r is around $n_r = 3.5$. There is a high-order magnetic mode around $\lambda = 1375$ nm, which is around the size of the cavity [Figs. 5(b)–5(d)]. This mode can be efficiently excited by a y-polarized MQE with a magnetic Purcell factor of $\Gamma^{sp}/\Gamma_0 \approx 1200$. The Q factor is about 1.5×10^3. On the other hand, if an EQE is placed at the same point, the Γ_e^{sp}/Γ_0^e for an EQE polarized in x, y, and z are only 2.5, 0.3 and 0.3, respectively. We take an average value of $\Gamma_e^{sp}/\Gamma_0^e \approx 1$ for an EQE. The ratio $\frac{\Gamma^{sp}/\Gamma_0}{\Gamma_e^{sp}/\Gamma_0^e}$ can reach $\sim 10^3$. This means that the magnetic interaction can exceed the electric one if Γ_0^e/Γ_0 of an emitter is smaller than $\sim 10^3$. $\frac{\Gamma^{sp}/\Gamma_0}{\Gamma_e^{sp}/\Gamma_0^e}$ increases exponentially with n_r and reaches $\sim 10^5$ around $n_r = 5$ [Fig. 5(e)]. Based on Eq. (6), the N_{MQE}^{th} for the above magnetic mode with $n_r = 3.5$ is $N_{MQE}^{th} \sim 10^6$. This number is achievable in such a system. The Q factor of the mode increases almost exponentially with n_r. Thus, the N_{MQE}^{th} decreases almost exponentially with n_r [Fig. 5(f)]. It is also relatively beneficial to enlarge the cavity size, and the discussion is the same as that in a WGM cavity (Fig. 2).

V. CONCLUSION

In conclusion, we have theoretically proposed that a magnetic laser can be obtained through the stimulated emissions of MQEs in a subwavelength dielectric cavity. The quantum treatment of such a hybrid system is carried out by considering the interactions of quantized magnetic field and two-level MQEs. The magnetic laser can be achieved in a subwavelength cavity based on the facts that the cavity can host high-Q electromagnetic resonances with significant magnetic near-field responses. The saturated number of photons N_n^{max} shows a linear relation with the pumping rate when the number of MQEs is more than several times larger than its threshold value. The competition between the electric interaction and
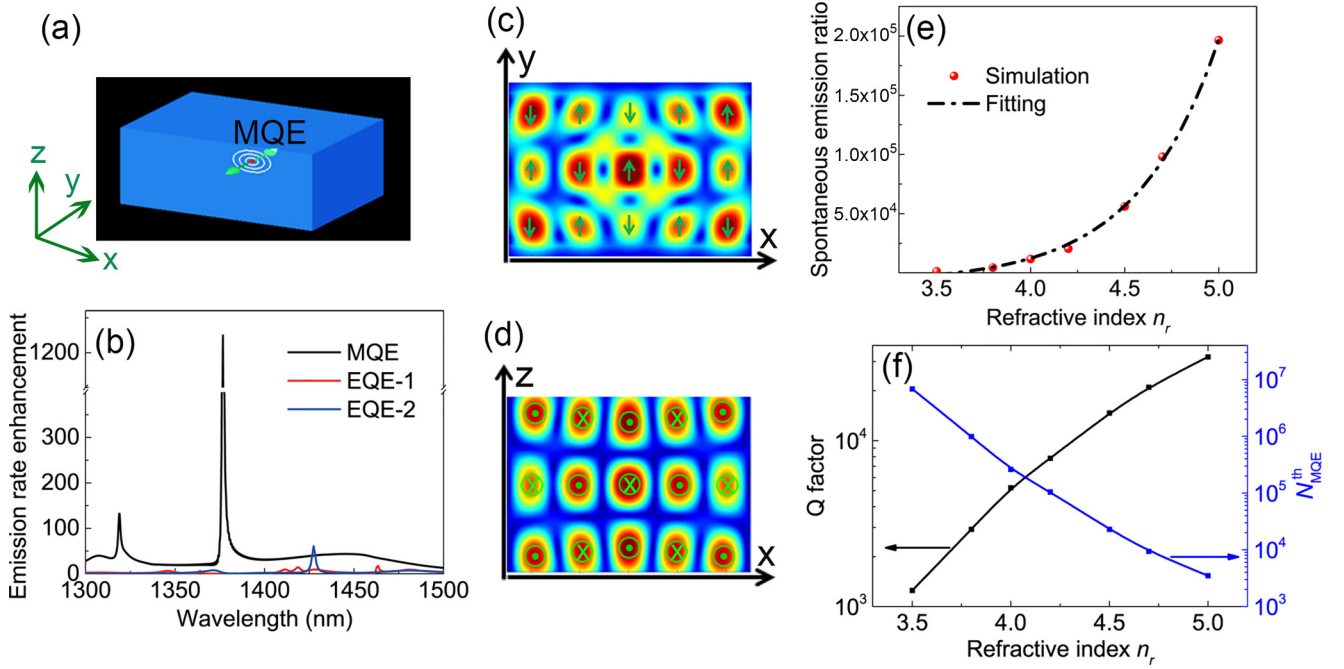
FIG. 5. (a) Schematic of a dielectric block excited by a MQE. The origin of the coordinate system is placed at the block center. (b) Spontaneous emission rate enhancement of a MQE ($\Gamma^{\mathrm{sp}}/\Gamma_0$) and an EQE ($\Gamma_e^{\mathrm{sp}}/\Gamma_0^e$). Polarization of the MQE is along y axis. Polarization of the EQE is along x axis (EQE-1) or z axis (EQE-2). Emitter is located at the block center in each case. $n_r = 3.5$. (c), (d) Magnetic field distribution on the x-y (c) and x-z (d) plane of the MQE-excited block at $\lambda = 1375$ nm. Arrows denote the main feature of the magnetic field directions. (e) Emission ratio $\frac{\Gamma^{\mathrm{sp}}/\Gamma_0}{\Gamma_e^{\mathrm{sp}}/\Gamma_0^e}$ as a function of the refractive index n_r. (f) Q factor and $N_{\mathrm{MQE}}^{\mathrm{th}}$ as a function of n_r. Size of the block in (e) and (f) is the same as that in (b).

magnetic one in terms of their decay-rate enhancements is also considered. In a wavelength-scale block cavity, their Purcell factor ratio can reach more than $\sim 10^3$ large ($n_r = 3.5$) due to the location-dependent emission properties. The widely developed fabrications of combined systems of dielectric structures and rare-earth ions may provide technical support for realizing our proposed magnetic laser in experiments [47–52]. It should be noted that to keep the couplings between MQEs and a cavity efficient enough in experiments, the MQEs should be placed carefully to match the near-field distributions of a cavity mode. Our results will enrich the laser field and could find important applications in enhanced magnetic light-matter interactions.

APPENDIX A: THE INTERACTION HAMILTONIAN BETWEEN A MQE AND THE QUANTIZED MAGNETIC FIELD OF A CAVITY

The magnetic field of a high-Q electromagnetic mode in a cavity can be expressed as

$$\vec{H}(r, t) = a\vec{Q}(r)\cos[\omega_n t + \varphi(r)]$$
$$= \frac{a}{2}\vec{Q}(r)e^{-i[\omega_n t + \varphi(r)]} + \frac{a}{2}\vec{Q}(r)e^{i[\omega_n t + \varphi(r)]}, \quad \text{(A1)}$$

where $\varphi(r)$ represents the spatial phase of the magnetic field, ω_n is the frequency of the photon, and a is the maximal magnitude of the magnetic field ($H_{\max}$), namely, $H_{\max} = a$. $\vec{Q}(r)$ is a real function of r. It represents the normalized magnitude of the magnetic at location r, and the maximal value of $\vec{Q}(r)$ is 1. Thus, the combination of $\vec{Q}(r)$ and a [namely, $a\vec{Q}(r)$] means the magnitude of magnetic field at location r [denoted by $\vec{H}(r)$]. Thus, we also have $\vec{Q}(r) = \vec{H}(r)/H_{\max} = \vec{B}(r)/B_{\max}$, where $\vec{B}(r) = \mu_0\vec{H}(r)$. The time-averaged energy of a magnetic mode can be expressed in terms of magnetic field as

$$U_m = \frac{1}{2}\int \mu_0|\vec{H}(r)|^2 d^3r$$
$$= c^2 a^2, \quad \text{(A2)}$$

where $c^2 = \frac{1}{2}\int \mu_0|\vec{Q}(r)|^2 d^3r$. The quantized Hamiltonian becomes the harmonic oscillator form [37,41,42] provided that $a = \frac{\sqrt{\hbar\omega_n}}{c}\hat{a}$ and $a^* = \frac{\sqrt{\hbar\omega_n}}{c}\hat{a}^+$. Here, $\hat{a}^+$ and $\hat{a}$ are the creation and annihilation operators of a photon, respectively. The quantized magnetic field as a function of position and time can be written as [37,41,42]

$$\vec{H}(r, t) = \frac{\sqrt{\hbar\omega_n}}{2c}\vec{Q}(r)\hat{a}e^{-i[\omega_n t + \varphi(r)]} + \frac{\sqrt{\hbar\omega_n}}{2c}\vec{Q}(r)\hat{a}^+e^{i[\omega_n t + \varphi(r)]}. \quad \text{(A3)}$$

The interaction Hamiltonian is $H_{\mathrm{int}} = -\vec{M}\cdot\vec{B}$, where $\vec{M}$ is the magnetic dipole moment of a MQE. With the second quantization and rotating-wave approximation [42], H_{int} can

be expressed as

$$
\begin{aligned}
H_{\text{int}} &= -\mu_0 \frac{\sqrt{\hbar \omega_n}}{c} \tilde{M}_{10} \cdot \vec{Q}(r)(\hat{a}\,\hat{\sigma}_{10} e^{-i[\omega_n t + \varphi(r)]} \\
&\quad + \hat{a}^+ \hat{\sigma}_{01} e^{i[\omega_n t + \varphi(r)]}) \\
&= -\hbar(\hat{a}\,\hat{\sigma}_{10} e^{-i[\omega_n t + \varphi(\vec{r})]} + \hat{a}^+ \hat{\sigma}_{01} e^{i[\omega_n t + \varphi(\vec{r})]}), \quad \text{(A4)}
\end{aligned}
$$

where $\tilde{M}_{10}$ is the matrix element of the MD transition, $\hat{\sigma}_{10} = |1\rangle\langle 0|$ and $\hat{\sigma}_{01} = |0\rangle\langle 1|$ are transition operators of a MQE, and g is the coupling strength

$$
\begin{aligned}
g &= \mu_0 \frac{\sqrt{\hbar \omega_n}}{2c} \tilde{M}_{10} \cdot \vec{Q}(r) \\
&= \mu_0 \frac{\sqrt{\hbar \omega_n}}{2c} \tilde{M}_{10} \cdot \frac{\vec{H}(r)}{H_{\max}} \\
&= \mu_0 \frac{\sqrt{\hbar \omega_n}}{2c} \tilde{M}_{10} \cdot \frac{\vec{B}(r)}{B_{\max}}. \quad \text{(A5)}
\end{aligned}
$$

The coupling strength g can also be written in terms of the mode volume of a magnetic mode. The mode volume of a magnetic mode can be expressed as

$$
\begin{aligned}
V_m &= \frac{\int \mu_0 |\vec{H}(r)|^2 \, d^3 r}{\mu_0 H_{\max}^2} \\
&= \frac{2c^2}{\mu_0}. \quad \text{(A6)}
\end{aligned}
$$

Based on Eqs. (A5) and (A6), the coupling strength g can also be written as

$$
g = \sqrt{\frac{\mu_0 \omega_n}{2\hbar V_m}} \tilde{M}_{10} \cdot \frac{\vec{B}(r)}{B_{\max}}. \quad \text{(A7)}
$$

APPENDIX B: STIMULATED EMISSION AND ABSORPTION RATE

Under Fermi's golden rule, the total emission rate into photons from a MQE can be expressed as

$$
\Gamma' = \frac{2\pi}{\hbar^2} |\langle N_n + 1, 0|H_{\text{int}}|N_n, 1\rangle|^2 \delta(\omega_{10} - \omega_n), \quad \text{(B1)}
$$

where ω_{10} is the frequency of MQE transition. $|N_n, 1\rangle$ represents a state where there are N_n photons and the MQE is on the excited state. Similarly, $|N_n + 1, 0\rangle$ represents a state where there are $N_n + 1$ photons and the MQE is on the ground state. Based on Eq. (A4), the magnitude matrix element for the emission of a photon can be written as

$$
|\langle N_n + 1, 0|H_{\text{int}}|N_n, 1\rangle| = \hbar\sqrt{N_n + 1}. \quad \text{(B2)}
$$

Considering certain spectral widths of both MQE transitions and photons [37], Eq. (B1) can be expressed as

$$
\Gamma' = 2\pi g^2 (N_n + 1) \int F(\omega) \frac{\gamma_n^2}{(\omega - \omega_n)^2 + \gamma_n^2} d\omega, \quad \text{(B3)}
$$

where $\int F(\omega) \frac{\gamma_n^2}{(\omega - \omega_n)^2 + \gamma_n^2} d\omega$ is the spectral overlap factor. $F(\omega)$ is the normalized-to-1 spectrum of MD transitions, and

γ_n is the relaxation rate of the photon. In the $N_n + 1$ term of Eq. (B3), the N_n represents the contribution from stimulated emission Γ^{st}, while the number 1 corresponds to the spontaneous emission Γ^{sp}. Similar to Eq. (B2), the magnitude matrix element for the absorption of a photon can be written as

$$
|\langle N_n - 1, 1|H_{\text{int}}|N_n, 0\rangle| = \hbar\sqrt{N_n}. \quad \text{(B4)}
$$

Thus, one can obtain the stimulated absorption rate Γ^{sa}, and it is equal to Γ^{st}.

APPENDIX C: THE RATE EQUATION FOR THE POPULATION OF MQES

The population density ρ_1 of MQEs at a given location satisfies

$$
\dot{\rho}_1 = \rho_0 W_{01} + \rho_0 \Gamma^{\text{st}} - \rho_1 \Gamma^{\text{st}} - \rho_1 \Gamma^{\text{sp}}, \quad \text{(C1)}
$$

where W_{01} is the pumping rate. Similarly, ρ_0 satisfies $\dot{\rho}_0 = -\dot{\rho}_1$. We can define $\rho_{\text{tot}} = \rho_1 + \rho_0$, and we also have $\rho_{\text{eff}} = \rho_1 - \rho_0$. Thus, $\dot{\rho}_{\text{eff}} = 2\dot{\rho}_1$. Then, ρ_1 and ρ_0 can be expressed as $2\rho_1 = \rho_{\text{tot}} + \rho_{\text{eff}}$ and $2\rho_0 = \rho_{\text{tot}} - \rho_{\text{eff}}$, respectively. Equation (C1) can be rewritten in terms of ρ_{eff} and ρ_{tot} as

$$
\dot{\rho}_{\text{eff}} = (W_{01} - \Gamma^{\text{sp}})\rho_{\text{tot}} - (W_{01} + \Gamma^{\text{sp}} + 2\Gamma^{\text{st}})\rho_{\text{eff}}. \quad \text{(C2)}
$$

Considering the integration over the whole region, one obtains Eq. (4).

APPENDIX D: THE STEADY-STATE SOLUTION FOR THE SATURATED NUMBER OF PHOTONS

The N_n^{max} can be obtained by solving Eqs. (3) and (4) under the steady-state conditions, namely, $\dot{\rho}_{\text{eff}} = 0$ and $\dot{N}_n = 0$. There are two solutions of N_n^{max}. The nagtive one is omitted. The positive one is

$$
\begin{aligned}
N_n^{max} &= \frac{1}{4} - \frac{W_{01}}{4\Gamma^{\text{sp}}} + \frac{W_{01} N_{\text{MQE}}}{4\gamma_n} \\
&\quad + \left[\frac{1}{16} + \frac{W_{01}}{8\Gamma^{\text{sp}}} + \frac{3W_{01} N_{\text{MQE}}}{8\gamma_n} \right. \\
&\quad \left. + \left(\frac{W_{01}}{4\Gamma^{\text{sp}}} - \frac{W_{01} N_{\text{MQE}}}{4\gamma_n} \right)^2 \right]^{1/2}. \quad \text{(D1)}
\end{aligned}
$$

When N_{MQE} is several times larger than $N_{\text{MQE}}^{\text{th}}(N_{\text{MQE}}^{\text{th}} = \frac{\gamma_n}{\Gamma^{\text{sp}}})$, the expression $[\frac{1}{16} + \frac{W_{01}}{8\Gamma^{\text{sp}}} + \frac{3W_{01} N_{\text{MQE}}}{8\gamma_n} + (\frac{W_{01}}{4\Gamma^{\text{sp}}} - \frac{W_{01} N_{\text{MQE}}}{4\gamma_n})^2]$ in Eq. (D1) is dominated by the $(\frac{W_{01}}{4\Gamma^{\text{sp}}} - \frac{W_{01} N_{\text{MQE}}}{4\gamma_n})^2$ term. Thus, the N_n^{max} becomes

$$
N_n^{max} \approx \frac{1}{4} + \frac{(N_{\text{MQE}} - N_{\text{MQE}}^{\text{th}})W_{01}}{2\Gamma^{\text{sp}}}. \quad \text{(D2)}
$$

When N_{MQE} is equal to N_{MQE}^{th}, the $\frac{W_{01}}{4\Gamma^{\text{sp}}} - \frac{W_{01} N_{\text{MQE}}}{4\gamma_n}$ term becomes 0. Thus, the N_n^{max} is

$$
N_n^{max} = \sqrt{\frac{W_{01}}{2\Gamma^{\text{sp}}} + \frac{1}{4}} - \frac{1}{4}, \quad \text{(D3)}
$$

namely, $N_n^{max} \propto \sqrt{\frac{W_{01}}{\Gamma^{\text{sp}}}}$.

[1] L. D. Landau and E. M. Lifshitz, *Electrodynamics of Continuous Media* (Pergamon Press, New York, 1984).

[2] H. Giessen and R. Vogelgesang, Glimpsing the weak magnetic field of light, Science **326**, 529 (2009).

[3] M. Burresi, D. van Oosten, T. Kampfrath, H. Schoenmaker, R. Heideman, A. Leinse, and L. Kuipers, Probing the magnetic field of light at optical frequencies, Science **326**, 550 (2009).

[4] D. G. Baranov, R. S. Savelev, S. V. Li, A. E. Krasnok, and A. Alu, Modifying magnetic dipole spontaneous emission with nanophotonic structures, Laser Photon. Rev. **11**, 1600268 (2017).

[5] B. R. Judd, Optical absorption intensities of rare-earth ions, Phys. Rev. **127**, 750 (1962).

[6] G. S. Ofelt, Intensities of crystal spectra of rare-earth ions, J. Chem. Phys. **37**, 511 (1962).

[7] C. M. Dodson and R. Zia, Magnetic dipole and electric quadrupole transitions in the trivalent lanthanide series: Calculated emission rates and oscillator strengths, Phys. Rev. B **86**, 125102 (2012).

[8] T. H. Taminiau, S. Karaveli, N. F. van Hulst, and R. Zia, Quantifying the magnetic nature of light emission, Nat. Commun. **3**, 979 (2012).

[9] M. Kasperczyk, S. Person, D. Ananias, L. D. Carlos, and L. Novotny, Excitation of Magnetic Dipole Transitions at Optical Frequencies, Phys. Rev. Lett. **114**, 163903 (2015).

[10] N. R. Brewer, Z. N. Buckholtz, Z. J. Simmons, E. A. Mueller, and D. D. Yavuz, Coherent Magnetic Response at Optical Frequencies Using Atomic Transitions, Phys. Rev. X **7**, 011005 (2017).

[11] S. Sun, D. Li, D. C. Wang, Z. Feng, W. Tan, and L. Wu, Empowering magnetic strong coupling and its application for nonlinear refractive index sensing, Nano Res. **15**, 7604 (2022).

[12] S. Karaveli and R. Zia, Spectral Tuning by Selective Enhancement of Electric and Magnetic Dipole Emission, Phys. Rev. Lett. **106**, 193004 (2011).

[13] M. Pelton, Modified spontaneous emission in nanophotonic structures, Nat. Photon. **9**, 427 (2015).

[14] L. Novotny and B. Hecht, *Principle of Nano-Optics* (Cambridge University Press, New York, 2006).

[15] E. M. Purcell, Spontaneous emission probabilities at radio frequencies, Phys. Rev. **69**, 681 (1946).

[16] S. M. Hein and H. Giessen, Tailoring Magnetic Dipole Emission with Plasmonic Split-Ring Resonators, Phys. Rev. Lett. **111**, 026803 (2013).

[17] R. Hussain, S. S. Kruk, C. E. Bonner, M. A. Noginov, I. Staude, Y. S. Kivshar, N. Noginova, and D. N. Neshev, Enhancing Eu3+ magnetic dipole emission by resonant plasmonic nanostructures, Opt. Lett. **40**, 1659 (2015).

[18] G. M. Pan, L. F. Yang, F. Z. Shu, Y. L. Meng, Z. Hong, and Z. J. Yang, Tailoring magnetic dipole emission by coupling to magnetic plasmonic anapole states, Photon. Res. **10**, 2032 (2022).

[19] A. I. Kuznetsov, A. E. Miroshnichenko, M. L. Brongersma, Y. S. Kivshar, and B. Luk'yanchuk, Optically resonant dielectric nanostructures, Science **354**, aag2472 (2016).

[20] Z. J. Yang, R. B. Jiang, X. L. Zhuo, Y. M. Xie, J. F. Wang, and H. Q. Lin, Dielectric nanoresonators for light manipulation, Phys. Rep. **701**, 1 (2017).

[21] T. H. Feng, Y. Xu, Z. X. Liang, and W. Zhang, All-dielectric hollow nanodisk for tailoring magnetic dipole emission, Opt. Lett. **41**, 5011 (2016).

[22] A. Vaskin, S. Mashhadi, M. Steinert, K. E. Chong, D. Keene, S. Nanz, A. Abass, E. Rusak, D. Y. Choi, I. Fernandez-Corbaton, T. Pertsch, C. Rockstuhl, M. A. Noginov, Y. S. Kivshar, D. N. Neshev, N. Noginova, and I. Staude, Manipulation of magnetic dipole emission from Eu $^{3+}$ with Mie-resonant dielectric metasurfaces, Nano Lett. **19**, 1015 (2019).

[23] M. Sanz-Paz, C. Ernandes, J. U. Esparza, G. W. Burr, N. F. van Hulst, A. Maitre, L. Aigouy, T. Gacoin, N. Bonod, M. F. Garcia-Parajo, S. Bidault, and M. Mivelle, Enhancing magnetic light emission with all-dielectric optical nanoantennas, Nano Lett. **18**, 3481 (2018).

[24] Q. Zhao, Z. J. Yang, and J. He, Coherent couplings between magnetic dipole transitions of quantum emitters and dielectric nanostructures, Photon. Res. **7**, 1142 (2019).

[25] K. Koshelev, S. Kruk, E. Melik-Gaykazyan, J. H. Choi, A. Bogdanov, H. G. Park, and Y. Kivshar, Subwavelength dielectric resonators for nonlinear nanophotonics, Science **367**, 288 (2020).

[26] Y. Q. Yang, V. A. Zenin, and S. I. Bozhevolnyi, Anapole-assisted strong field enhancement in individual all-dielectric nanostructures, ACS Photon. **5**, 1960 (2018).

[27] A. E. Miroshnichenko, A. B. Evlyukhin, Y. F. Yu, R. M. Bakker, A. Chipouline, A. I. Kuznetsov, B. Luk'yanchuk, B. N. Chichkov, and Y. S. Kivshar, Nonradiating anapole modes in dielectric nanoparticles, Nat. Commun. **6**, 8069 (2015).

[28] L. J. Huang, L. Xu, M. Rahmani, D. Neshev, and A. E. Miroshnichenko, Pushing the limit of high-Q mode of a single dielectric nanocavity, Adv. Photon. **3**, 016004 (2021).

[29] X.-J. Du, Z.-J. Yang, M.-L. Hu, L. Ma, and J. He, Ultrahigh electric and magnetic near field enhancement based on high-Q whispering gallery modes in subwavelength all-dielectric resonators, Appl. Phys. Express **14**, 082004 (2021).

[30] M. L. Hu, Z. J. Yang, X. J. Du, L. Ma, and J. He, Strong couplings between magnetic quantum emitters and subwavelength all-dielectric resonators with whispering gallery modes, Opt. Express **29**, 26028 (2021).

[31] M.-L. Hu, X.-J. Du, L. Ma, J. He, and Z.-J. Yang, Strong superradiance of coherently coupled magnetic dipole emitters mediated by whispering gallery modes of a subwavelength all-dielectric cavity, Phys. Rev. B **106**, 205420 (2022).

[32] L. N. He, S. K. Ozdemir, and L. Yang, Whispering gallery microcavity lasers, Laser Photon. Rev. **7**, 60 (2013).

[33] Q. J. Wang, C. L. Yan, N. F. Yu, J. Unterhinninghofen, J. Wiersig, C. Pflugl, L. Diehl, T. Edamura, M. Yamanishi, H. Kan, and F. Capasso, Whispering-gallery mode resonators for highly unidirectional laser action, Proc. Natl. Acad. Sci. USA **107**, 22407 (2010).

[34] X. F. Jiang, C. L. Zou, L. Wang, Q. H. Gong, and Y. F. Xiao, Whispering-gallery microcavities with unidirectional laser emission, Laser Photon. Rev. **10**, 40 (2016).

[35] P. Berini and I. De Leon, Surface plasmon-polariton amplifiers and lasers, Nat. Photon. **6**, 16 (2012).

[36] R. M. Ma, R. F. Oulton, V. J. Sorger, and X. Zhang, Plasmon lasers: Coherent light source at molecular scales, Laser Photon. Rev. **7**, 1 (2013).

[37] D. J. Bergman and M. I. Stockman, Surface Plasmon Amplification by Stimulated Emission of Radiation: Quantum Generation

of Coherent Surface Plasmons in Nanosystems, Phys. Rev. Lett. **90**, 027402 (2003).

[38] T. V. Shahbazyan, Mode volume energy transfer, and spaser threshold in plasmonic systems with gain, ACS Photon. **4**, 1003 (2017).

[39] O. Svelto and D. Hanna, *Principles of Lasers* (Springer, New York, 2014).

[40] D. G. Baranov, A. P. Vinogradov, A. A. Lisyansky, Y. M. Strelniker, and D. J. Bergman, Magneto-optical spaser, Opt. Lett. **38**, 2002 (2013).

[41] P. W. Milonni, Field quantization and radiative processes in dispersive dielectric media, J. Mod. Opt. **42**, 1991 (1995).

[42] R. Loudon, *The Quantum Theory of Light* (Oxford University Press, London, 1973).

[43] C. Sauvan, J. P. Hugonin, I. S. Maksymov, and P. Lalanne, Theory of the Spontaneous Optical Emission of Nanosize Photonic and Plasmon Resonators, Phys. Rev. Lett. **110**, 237401 (2013).

[44] J. Flick, N. Rivera, and P. Narang, Strong light-matter coupling in quantum chemistry and quantum photonics, Nanophotonics **7**, 1479 (2018).

[45] T. Yoshie, A. Scherer, J. Hendrickson, G. Khitrova, H. M. Gibbs, G. Rupper, C. Ell, O. B. Shchekin, and D. G. Deppe, Vacuum Rabi splitting with a single quantum dot in a photonic crystal nanocavity, Nature (London) **432**, 200 (2004).

[46] R. Miller, T. E. Northup, K. M. Birnbaum, A. Boca, A. D. Boozer, and H. J. Kimble, Trapped atoms in cavity QED: Coupling quantized light and matter, J. Phys. B:At. Mol. Opt. Phys. **38**, S551 (2005).

[47] A. Gritsch, L. Weiss, J. Fruh, S. Rinner, and A. Reiserer, Narrow Optical Transitions in Erbium-Implanted Silicon Waveguides, Phys. Rev. X **12**, 041009 (2022).

[48] P. Chen, J. P. Zhang, B. B. Xu, X. W. Sang, W. B. Chen, X. F. Liu, J. B. Han, and J. R. Qiu, Lanthanide doped nanoparticles as remote sensors for magnetic fields, Nanoscale **6**, 11002 (2014).

[49] B. Jiang, S. Zhu, W. Y. Wang, J. Li, C. H. Dong, L. Shi, and X. L. Zhang, Room-temperature continuous-wave upconversion white microlaser using a rare-earth-doped microcavity, ACS Photon. **9**, 2956 (2022).

[50] R. Emmanuele, M. Maciejczyk, A. Smith, X. Y. Cheng, E. Masson, D. J. Gosztola, S. W. Hla, N. Robertson, and X. D. Ma, Microcavity-modified emission from rare-earth ion-based molecular complexes, ACS Photon. **9**, 2315 (2022).

[51] Z. Chen, G. Dong, G. Barillaro, J. Qiu, and Z. Yang, Emerging and perspectives in microlasers based on rare-earth ions activated micro-/nanomaterials, Prog. Mater. Sci. **121**, 100814 (2021).

[52] X. Z. Cheng, X. L. Zhuo, R. B. Jiang, Z. G. Wang, J. F. Wang, and H. Q. Lin, Electromagnetic resonance-modulated magnetic emission in europium-doped sub-micrometer zirconia spheres, Adv. Opt. Mater. **9**, 2002212 (2021).